# C 1$s$ and N 1$s$ core excitation of aniline: Experiment by electron impact and *ab initio* calculations

D. Duflot and J.-P. Flament

*Laboratoire de Physique des Lasers, Atomes et Molécules (PhLAM), UMR CNRS 8523, Centre d'Études et de Recherches Lasers et Applications (CERLA, FR CNRS 2416), Université des Sciences et Technologies de Lille, F-59655 Villeneuve d'Ascq Cedex, France*

A. Giuliani

*DISCO Beamline, SOLEIL Synchrotron, BP 48, L'Orme des Merisiers, 91192 Gif-sur-Yvette Cedex, France*
*and Cepia, Institut National de la Recherche Agronomique, BP 71627, 44316 Nantes Cedex 3, France*

J. Heinesch, M. Grogna, and M.-J. Hubin-Franskin

*Laboratoire de Spectroscopie d'Électrons diffusés, Université de Liège, Institut de Chimie B6c, B-4000 Liège 1, Belgium*

Core shell excitation spectra of aniline at the carbon and nitrogen 1$s$ edges have been obtained by inner-shell electron energy-loss spectroscopy recorded under scattering conditions where electric dipolar conditions dominate, with higher resolution than in the previous studies. They are interpreted with the aid of *ab initio* configuration interaction calculations. The spectrum at the C 1$s$ edge is dominated by an intense $\pi^*$ band. The calculated chemical shift due to the different chemical environment at the carbon 1$s$ edge calculated is in agreement with the experimental observations within a few tenths of an eV. The transition energies of the most intense bands in the C 1$s$ excitation spectrum are discussed at different levels of calculations. In the nitrogen 1$s$ excitation spectrum the most intense bands are due to Rydberg-valence transitions involving the $\sigma^*$-type molecular orbitals, in agreement with the experiment. This assignment is different from that of extended Hückel molecular orbital calculations. The geometries of the core excited states have been calculated and compared to their equivalent core molecules and benzene.

PACS number(s): 32.80.Hd, 34.80.Gs

## I. INTRODUCTION

One of the most important properties of aniline is to polymerize easily in polyaniline. This polymer is relatively easy to synthesize and can get, under specific conditions, interesting electric conducting properties [1]. This is also involved for the synthesis of molecular systems having potentially large nonlinear optical responses [2].

The physicochemical properties of polyaniline are related at least partly to the $\pi$ molecular orbitals in the valence bands but also in the empty levels. In a general way these are expected at least for thin films to be predicted to be not too different from the individual molecule constituting the unit.

To our knowledge core excitation spectra of aniline have been reported by only two experimental studies previously, namely x-ray photoabsorption [near-edge x-ray-absorption fine-structure (NEXAFS)] of the condensed multilayer solid [3–5] and inner-shell electron energy-loss spectroscopy (ISEELS) of aniline in gas phase [6]. Calculations of the core excitation spectra have been reported using the extended Hückel molecular orbital (EHMO) method [6], the multiconfiguration self-consistent-field (MCSCF) method for the carbon first $\pi^*$ transitions [5], and the static exchange (STEX) method [7,8]. In Ref. [7], the assignments of the main features of the spectra were briefly discussed, while in the later work, no detailed discussion was given.

In the present work the electronic structure of aniline, and much more specifically the unoccupied levels, have been investigated by core shell excitation and *ab initio* calculations. Inner-shell electron energy-loss spectroscopy has been used to record the C 1$s$ and N 1$s$ excitation spectra of aniline. The experimental conditions—high electron impact energy and

quite small scattering angle—are such that electron energy-loss spectra are expected to exhibit the same features with quite similar relative intensities to those of the corresponding ones in photoabsorption.

The core excitation spectra have been measured for gaseous aniline with higher energy resolution than in the previous studies. *Ab initio* configuration interaction (CI) calculations have been performed to assist in the spectral assignments and to discuss aspects of the unoccupied molecular-orbital electronic structure.

## II. EXPERIMENTAL PART

The inner-shell electron energy-loss spectra were obtained with a Vacuum Science Workshop Ltd. spectrometer which has been adapted for gas studies and high-energy electron beams and has been equipped with a home-made position sensitive multidetector system in order to improve data collection times. The experimental apparatus and procedure have been described in detail previously [9–11].

Briefly the spectrometer consists of an electrostatic 180° monochromator operating in the constant pass energy mode, a collision chamber, and an electrostatic analyzer identical to the monochromator. The monochromatized incident electrons are accelerated up to 2 keV and focused into the collision chamber using a four-element electron lens. The electrons are slightly deflected (0.02 radians) by two sets of $X$-$Y$ plates inside the collision chamber. The scattered electrons are energy analyzed and focused onto the entrance slit of the analyzer by a lens similar to that used for acceleration.

In the collision conditions of quite low momentum transfer (i.e., high incident energy and quite small scattering

angle), only electronic electric-dipolar transitions are excited. Inside the vacuum vessel, a residual pressure of less than $1 \times 10^{-8}$ Torr is maintained by a cryogenic pumping system. The electron gun and the analyzer regions are differentially pumped by turbomolecular pumps, respectively. The spectra have been recorded with 0.040- and 0.020-eV steps.

In order to take into account valence and lower-energy inner-shell excitation cross section, a linear background has been subtracted from the raw spectra by extrapolating a least-square fit of the pre-edge experimental data points.

The absolute energy scale has been calibrated at both edges relative to CO and the C $1s \to \pi^*$ ($\nu'=0$) band at $287.40 \pm 0.02$ eV [12] recording the spectra with 0.01-eV steps and the mean value of $400.99 \pm 0.09$ eV between the N $1s \to \pi^*$ ($\nu'=0$) at 400.88 eV and the N $1s \to \pi^*$ ($\nu'=1$) at 401.1 eV [12] recording the spectra with 0.02-eV steps.

The sample has been provided by ACROS Organics with a stated purity better than 99.5%. It was used directly without further purification except for repetitive freeze-pump-thaw cycles in order to eliminate air and other volatile impurities in the sample.

## III. COMPUTATIONAL METHOD

Since the computational method used has been described in detail elsewhere [13], it will be briefly outlined. The starting hypothesis [14] is that, due to the important relaxation of the electronic density following the creation of the core hole, the molecular orbitals (MOs) of the core *ionized* molecule are a better approximation for the description of the core *excited* states than the ground state MOs. Formally, the energy of a given $1s \to i^*$ core excited state may be obtained by correcting the core ion energy in the following manner:

$$E(1s \to \mathbf{i}^*) = E(1s \to \infty) + \varepsilon_{\mathbf{i}^*} + P_{\mathbf{i}^*} + C_{\mathbf{i}^*},$$

where $\varepsilon_{\mathbf{i}^*}$ is the Hartree-Fock monoelectronic energy of the $i^*$ MO. $E(1s \to \infty)$ is the core ion energy, obtained using the ROHF-GVB method implemented in the GAMESS-US package [15]. The $P_{\mathbf{i}^*}$ and $C_{\mathbf{i}^*}$ terms represent the residual relaxation and valence correlation effects of the $i^*$ electron with respect to the core ion, respectively. The relaxation term is taken into account by performing a configuration interaction (CI) calculation in the monoexcitation space of the lowest-lying core states, obtained by a preliminary diagonalization of the full $1s \to i^*$ CI matrix. In order to evaluate the $C_{\mathbf{i}^*}$ term, the calculated CI wave functions serve as the zeroth-order space for a multireference MP2 calculation using the three-class diagrammatic CIPSI method [16,17]. To spare computational time, an extrapolation procedure [18] was employed, using six thresholds between 97.0 and 99.5 % of the exact wave functions. Finally, the dipolar electric transition oscillator strengths with respect to the ground state of the molecule were computed, using the length gauge.

The Gaussian atomic orbitals (AOs) used are the TZP basis set taken from Dunning [19]. For the calculation of the core excited states, a set of Rydberg orbitals ($5s, 5p, 2d$) was added to the core excited atom basis set. The first exponents were taken from Dunning and Hay [20] and the last ones

were determined in an "even-tempered" manner. In the following, the basis set with diffuse functions will be named " TZP+$R$." The theoretical width of the bands was set to the experimental resolution (0.17 eV) and a Gaussian profile was used in the comparison of the calculations and the experiment.

The aniline molecule contains four chemically nonequivalent carbons and one nitrogen atom (see Fig. 1 for labeling). For the calculation of the core ionized MOs at both edges, core hole localization was assumed and the coupling between excitations from different core holes was neglected.

## IV. RESULTS AND DISCUSSION

It is now well known that aniline is nonplanar in its ground electronic state [21,22], the amine group being pyramidally distorted [Fig. 1(a)]. The symmetry point group is therefore $C_s$, with the symmetry plane corresponding to the ($yz$) plane using the frame of Fig. 1(a). The energy difference between the planar [Fig. 1(a)] and nonplanar [Fig. 1(c)] conformations is rather small, with proposed values of 524.4 cm$^{-1}$ [23], 454 cm$^{-1}$ [24], and 509.0 cm$^{-1}$ [25]. From the theoretical point of view, this quantity is very sensitive to the basis set and method employed [26,27]. In the present work, the inversion barrier is calculated to be 388 cm$^{-1}$ at the HF level and 710 cm$^{-1}$ at the MP2 level.

In the present work, as in previous theoretical studies of core excited aniline [5,6,8], the planar conformation was used. This geometry reduces the computational cost and allows calculating a larger number of states. Moreover, the high symmetry facilitates the assignment of the core states. The calculation of valence electronic spectrum for nonplanar and planar conformations [28] showed very small differences for the energies and intensities (Fig. 3 of [28]). Therefore for N and $C_4$ atoms, the calculations were performed in the $C_{2v}$ group of planar aniline. For $C_2$ and $C_3$, because of assumed core hole localization, the $C_{2v}$ symmetry was reduced to $C_s$, but with the symmetry plane being the ($xz$) plane of Fig. 1. Thus it should be kept in mind that the ($xz$) symmetry plane used for $C_2$ and $C_3$ is in fact perpendicular to the true ($yz$) symmetry plane of the molecule, resulting in an inversion between $A'$ and $A''$ irreducible representations.

The use of $C_{2v}$ symmetry also has some consequences on the allowed dipole electric transitions: the $1s(a_1) \to \pi^*(a_2)$ or $nd(a_2)$ transitions are forbidden while all transitions should be allowed in the nonplanar ($C_s$) conformation. However, their intensities should be small when compared to other transitions.

The calculated HF electronic configuration of the neutral ground state of aniline for the planar molecule is

$$1a_1^2 2a_1^2 3a_1^2 1b_2^2 2b_2^2 4a_1^2 5a_1^2 6a_1^2 7a_1^2 3b_2^2 8a_1^2 4b_2^2 9a_1^2$$
$$\times 10a_1^2 5b_2^2 11a_1^2 12a_1^2 6b_2^2 7b_2^2 1b_1^2 13a_1^2 8b_2^2 2b_1^2 1a_2^2 3b_1^2.$$

The seven first MO's (molecular orbitals) are the $1s$ orbitals of the nitrogen atom and of the six carbon atoms. There are four occupied $\pi$-type MO's, namely the $1b_1$, $2b_1$, $1a_2$, and $3b_1$. The $1b_1$ MO corresponds to the nitrogen lone pair, with $C_1$ and $C_2$ bonding character; the $2b_1(1\pi)$ MO has
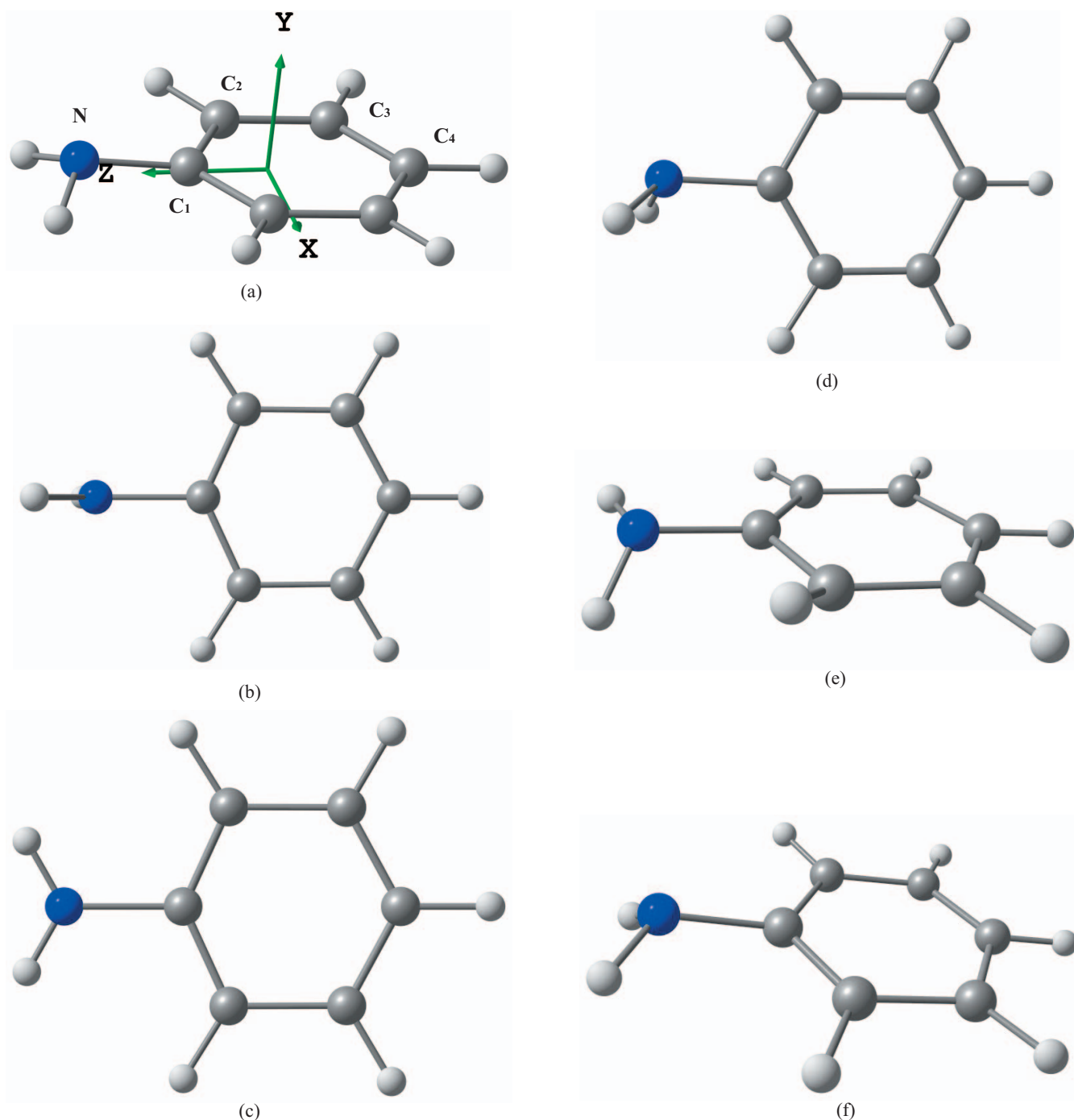
FIG. 1. (Color online) (a) Labeling of atoms in aniline and ground-state geometry. (b)–(f) Possible geometries for core ionized and excited states of aniline and their $Z+1$ equivalent.

$C_3$-$C_4$ bonding character, and antibonding with the N lone pair; the $1a_2(2\pi)$ is essentially the $\pi(C_2$-$C_3)$ MO and finally, the $3b_1(3\pi,\text{HOMO})$ has $C_3$-$C_4$ and $C_1$-$C_2$ bonding character, with $C_2$-$C_3$ and $C_1$-N antibonding character. There are three unoccupied $\pi^*$ MO's: $2a_2$ ($1\pi^*$, lowest unoccupied molecular orbital), $4b_1$ ($2\pi^*$), and $5b_1$ ($3\pi^*$) (see Fig. 8 of Ref. [3]).

The HF and MP2 optimized geometries of the ground state, obtained for both $C_{2v}$ and $C_s$ conformations, are compared with previous experimental [22] and theoretical [29]

works in the supplementary data of this paper [30] (see also [27]). The $C_s$ MP2 results agree quite well with the experiment. The pyramidalization of the amine group is usually measured via the $\phi$ angle between the H-N-H bisector axis and the $C_1C_4$ axis. Our calculated MP2 $\phi$ value of 41.41° is slightly larger than the earlier measures (37.5° in [22]), partly due to the fact that in some previous studies, the N, $C_1$, and $C_4$ atoms were supposed to be aligned. Other determinations are very close to our calculations: 42.17° in [23], 42° in [24], and 41.7° in [25].

TABLE I. Core ionization energies (eV) of aniline at the N 1*s* and C 1*s* edges.

| | $\Delta$SCF[a] | Shift[a] | $\Delta$MP2 (CIPSI)[b] | Shift[b] | $\Delta$MP2 (ZAPT)[b] | Shift[b] | $\Delta$MP2 (RMP)[b] | Shift[b] | $\Delta$SCF[c] | Shift[c] | STEX[d] | Shift[d] | Expt.[e] | Shift[e] |
|---|---|---|---|---|---|---|---|---|---|---|---|---|---|---|
| $C_1$ | 291.77 | 2.00 | 291.52 | 1.73 | 291.64 | 1.74 | 291.62 | 1.73 | 291.77 | 2.00 | 291.53 | 1.92 | 291.3 | 1.6 |
| $C_2$ | 289.94 | 0.17 | 289.99 | 0.20 | 290.11 | 0.21 | 290.09 | 0.20 | 289.96 | 0.19 | 289.77 | 0.16 | 289.9 | 0.2 |
| $C_3$ | 290.39 | 0.62 | 290.13 | 0.34 | 290.24 | 0.34 | 290.23 | 0.34 | 290.41 | 0.64 | 290.31 | 0.70 | 290.2 | 0.5 |
| $C_4$ | 289.77 | 0.00 | 289.79 | 0.00 | 289.90 | 0.00 | 289.89 | 0.00 | 289.77 | 0.00 | 289.61 | 0.00 | 289.7 | 0.0 |
| N | 405.30 | | 405.47 | | 405.60 | | 405.59 | | 405.30 | | 405.41 | | 405.3 | |

[a]This work. Gas phase values calculated at the TZP/RHF optimized geometry using the TZP+Rydberg basis set.
[b]This work. Gas phase values calculated at the TZP/MP2 optimized geometry using the TZP+Rydberg basis set.
[c]Reference [8].
[d]Reference [7].
[e]Reference [31].

### A. Core ionization energies

The calculated core ionization energies obtained at the $\Delta$MP2 and $\Delta$SCF levels are given in Table I and compared with the $\Delta$SCF results of Carravetta *et al.* [8] and the XPS experimental values [31]. Since in MP2 calculations, several possible definitions of the zero-order Hamiltonian for open-shell systems are possible [32], the $\Delta$MP2 values of the present work were obtained using three different models: RMP [33,34], ZAPT [35,36], and CIPSI. The two $\Delta$SCF are nearly identical because Carravetta *et al.* [8] employed the same basis set as in the present work. While RMP and ZAPT methods are very similar, the CIPSI values are slightly different. All results are within 0.5 eV of the experimental values.

In order to test the influence of using a planar geometry on core energies, the calculations were done in both planar ($C_{2v}$) and nonplanar ($C_s$) conformations. As shown in the EPAPS document [30], using the nonplanar geometry affects the core ionization energies by at most 0.18 eV, although the variation is different for each atom. For carbon atoms, the nonplanar absolute energy values are closer to experiment

than the planar results. The situation is reversed for nitrogen. Globally, for both geometries, chemical shifts are in good agreement with experiment, while most calculated absolute energies are too large by a few tenths of an eV. A similar trend will be found in the calculation of the core excitation spectra (see next sections). In order to remain consistent with the calculation of the core excited states, the CIPSI values obtained in the planar geometry will be used as a reference in the following.

### B. Nitrogen *K*-shell electron energy-loss spectrum

The electron energy-loss spectrum measured experimentally at the N 1*s* edge is displayed in Fig. 2. The lowest energy bands are a little bit better resolved than in previous work [6] thanks to the higher resolution in the present study. The energies are given in Table II and are in excellent agreement with those obtained by Turci *et al.* [6]. Table II gives also the assignments proposed by Turci *et al.* [6]. The results of the calculations are given in Table III. Only the transitions with intensities larger than 1.5% of the most intense band are shown, except for $A_2$ transitions. As for the core ionization
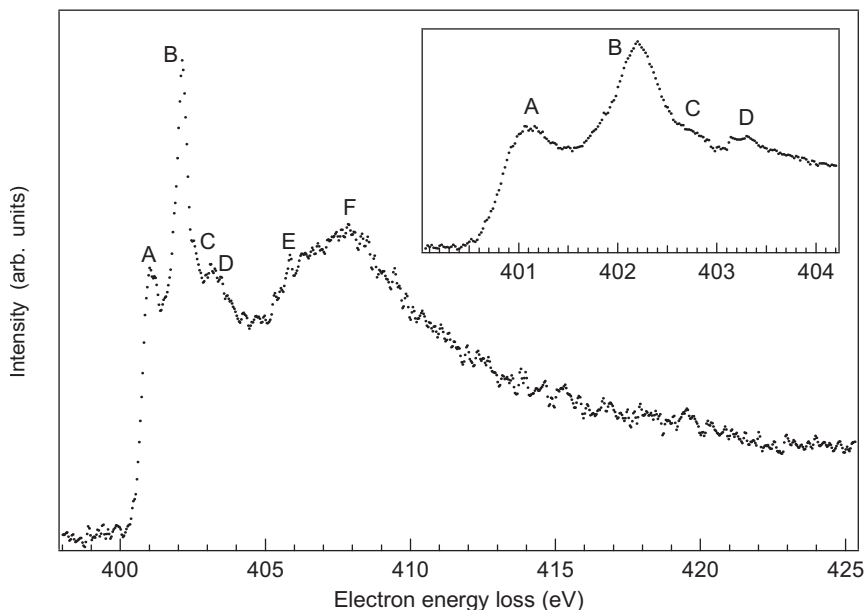


FIG. 2. The electron energy-loss spectrum aniline recorded at the nitrogen *K*-edge with an energy resolution of 0.17 eV, steps of 40 meV. Inset: lowest energy region recorded with 20-meV steps.

TABLE II. Experimental energy values (eV) of the spectral bands in the N 1s excitation spectrum of aniline and previous proposed assignments.

| Band | $E$ (eV)[a] | TV (eV)[b] | $E$ (eV)[c] | TV (eV)[c] | Assignment[c] |
|------|------|------|------|------|------|
| A | 401.1 | 4.2 | 400.7 | 4.6 | $3s$ |
| B | 402.2 | 3.1 | 402.2 | 3.1 | $3p/\pi^*$ (NH$_2$) $(2\pi^*, 4b_1)$ |
| C | 402.72 | 2.58 | | | |
| D | 403.24 | 2.06 | 404 | 1.3 | $\sigma^*$ (NH$_2$) |
| E | 406.1 | −0.8 | | | |
| F | 407.6 | −2.3 | 407.6 | −2.3 | $\sigma^*$ (CN) |

[a]This work.
[b]This work using ionization energy of Ref. [31].
[c]Reference [6].

energy, the calculated values seem to be overestimated by a few tenths of an eV. This implies that the calculated term values (TV's) should be in better agreement with experiment than the absolute energies. Therefore TV's of Tables II and III will be used for the assignment of the spectrum.

The first band A is observed at 401.1 eV (TV=4.2 eV) and is only partly resolved from the most intense one. It was assigned by Turci *et al.* [6] to the N 1s→3s transition. Plash-

kevych *et al.* [7] suggested $p\sigma^*$ ($a_1$) MO with $s$ character. As shown in Table III, the calculations confirm partially this assignment: the N 1s→3s$\sigma$/$\sigma^*$ (NH$_2$) transition is calculated at 401.49 eV (TV=3.98 eV) but its rather large intensity is due to the important $\sigma^*$ (NH$_2$) valence character of the 3s Rydberg orbital.

The next band B is located at 402.2 eV (TV=3.1 eV) and was assigned to the N 1s→3p/$\pi^*$ (NH$_2$) $(2\pi^*, 4b_1)$ transi-

TABLE III. Calculated energies, term values (TV), relative intensities, and assignments of N 1s core excited states of aniline.

| State | $E$ (eV) | TV (eV) | Intensity[a] | Main configurations[b] | $\langle r^2 \rangle$ |
|-------|------|------|------|------|------|
| $A_1$ | 401.49 | 3.98 | 0.114 | 0.97 N 1s→3s$\sigma$/$\sigma^*$ (NH$_2$) | 133 |
| $B_2$ | 402.53 | 2.94 | 0.465 | 0.97 N 1s→3p$\sigma$/$\sigma^*$ (NH$_2$) | 144 |
| $A_2$ | 402.60 | 2.87 | 0.000[c] | 0.45 N 1s→1$\pi^*$ ($2a_2$) | 86 |
| | | | | +0.43 N 1s→3d$\pi$ | |
| $B_1$ | 402.61 | 2.86 | 0.171 | 0.54 N 1s→2$\pi^*$ ($4b_1$) | 89 |
| | | | | +0.24 N 1s→3p$\pi$ | |
| | | | | +0.11 N 1s→4p$\pi$/2$\pi^*$ | |
| $B_1$ | 403.26 | 2.21 | 0.281 | 0.74 N 1s→3p$\pi$ | 181 |
| | | | | +0.17 N 1s→2$\pi^*$ ($4b_1$) | |
| $A_1$ | 403.66 | 1.81 | 0.024 | 0.95 N 1s→4s$\sigma$ | 309 |
| $B_2$ | 403.73 | 1.73 | 0.086 | 0.98 N 1s→3d$\sigma$/$\sigma^*$ (NH$_2$) | 244 |
| $A_2$ | 403.98 | 1.49 | 0.000[c] | 0.54 N 1s→3d$\pi$ | 274 |
| | | | | +0.43 N 1s→1$\pi^*$ ($2a_2$) | |
| $B_1$ | 403.99 | 1.47 | 0.023 | 0.96 N 1s→3d$\pi$ | 275 |
| $B_2$ | 404.09 | 1.38 | 0.072 | 0.98 N 1s→4p$\sigma$/$\sigma^*$ (NH$_2$) | 432 |
| $B_1$ | 404.26 | 1.21 | 0.098 | 0.77 N 1s→4p$\pi$/2$\pi^*$ ($4b_1$) | 524 |
| $A_2$ | 404.52 | 0.94 | 0.000[c] | 0.90 N 1s→4d$\pi$ | 589 |
| $B_1$ | 404.64 | 0.83 | 0.036 | 0.92 N 1s→5p$\pi$ | 985 |
| | 405.47 | 0.00 | | Ion | |
| $A_1$ | 405.47 | 0.00 | 0.123 | 096 N 1s→$\sigma^*$ (NH$_2$) | 274 |
| $B_2$ | 405.56 | −0.09 | 1.000[d] | 0.96 N 1s→$\sigma^*$ (NH$_2$) | 220 |
| $B_1$ | 406.60 | −1.13 | 0.033 | 0.56 N 1s→3$\pi^*$ ($5b_1$) | 110 |
| $B_2$ | 406.90 | −1.43 | 0.034 | 0.80 N 1s→$\sigma^*$ (C$_3$H) | 147 |

[a]Relative intensity to the most intense band.
[b]Main configuration of the CI wave function.
[c]Dipole-electric forbidden transition.
[d]Absolute calculated oscillator strengths (length gauge): $f_L$=0.0199.

TABLE IV. Quantum defect analysis (energies in eV).

| | N | | | $C_1$ | | | $C_2$ | | | $C_3$ | | | $C_4$ | |
|---|---|---|---|---|---|---|---|---|---|---|---|---|---|---|
| | $\delta_\ell$ | IP | | $\delta_\ell$ | IP | | $\delta_\ell$ | IP | | $\delta_\ell$ | IP | | $\delta_\ell$ | IP |
| $ns(a_1)$ | 1.14 | 405.42 | $ns(a_1)$ | 0.84 | 291.41 | $ns(a')$ | 0.97 | 290.12 | $ns(a')$ | 0.94 | 290.25 | $ns(a_1)$ | 0.83 | 289.69 |
| $np(a_1)$ | 0.56 | 405.45 | $np(a_1)$ | 0.60 | 291.47 | $np(a')$ | 0.71 | 290.07 | $np(a')$ | 0.70 | 290.21 | $np(a_1)$ | 0.65 | 289.71 |
| $np(b_2)$ | 0.84 | 405.45 | $np(b_2)$ | 0.58 | 291.42 | $np(a')$ | 0.68 | 290.14 | $np(a')$ | 0.67 | 290.27 | $np(b_2)$ | 0.48 | 289.66 |
| $np(b_1)$ | 0.48 | 405.38 | $np(b_1)$ | 0.32 | 291.40 | $np(a'')$ | 0.35 | 289.83 | $np(a'')$ | 0.43 | 290.07 | $np(b_1)$ | 0.33 | 289.65 |
| CIPSI | | 405.47 | | | 291.52 | | | 289.99 | | | 290.13 | | | 289.79 |

tion by Turci *et al.* [6] and to a $p\sigma^*$ ($b_2$) MO by Plashkevych *et al.* [7]. The present calculations of Table III show a much more complex situation, since there are three transitions predicted to have a TV around 2.9 eV. The most intense one, calculated at 402.53 eV (TV=2.94 eV), is due to the N $1s$ $\rightarrow 3p\sigma/\sigma^*$ (NH$_2$), i.e., an in-plane $3p\sigma$ with an important $\sigma^*$ (NH$_2$) valence character. The two other states are nearly degenerate and correspond to transitions to the $1\pi^*$ ($2a_2$) and $2\pi^*$ ($4b_1$) MO's. For both states, the CI wave functions appear to be a mixing between $\pi^*$ and Rydberg MO's ($3d\pi$ for $1\pi^*$ and $3p\pi/4p\pi$ for $2\pi^*$). However, the low values of the $\langle r^2 \rangle$ parameters (86 and 89 a.u.$^2$) prove without ambiguity the two transitions to have a valence character and corresponding to the $1\pi^*$ ($2a_2$) and $2\pi^*$ ($4b_1$) transitions. It should also be noticed that if the nonplanar geometry had been used, the $A_2$ transition would have $A''$ symmetry while the $B_1$ transition would be $A'$. The $A_2$ transition would then be allowed but its intensity should be weak. Experimentally, the $\sigma/\pi$ nature of band $B$ could be confirmed by measuring the near-edge x-ray-absorption fine-structure spectra of condensed aniline at glancing and normal incidence [4], as done at the C $1s$ edge [3], or by using the symmetry-resolved method of Shigemasa *et al.* [37].

A shoulder $C$ not well resolved on the high-energy side of the most intense band is observed at 402.72 eV (inset of Fig. 2, Table II), corresponding to a TV of 2.58 eV. According to the data of Table IV, it involves excitation to the $3p\pi$ MO, calculated at 403.26 eV (TV=2.30 eV). While the $\langle r^2 \rangle$ value of 181 a.u.$^2$ identifies this transition to be of Rydberg character, its unusually high intensity (28.1% of the most intense band) may be explained by a mixing with the N $1s \rightarrow 2\pi^*$ ($4b_1$) excitation.

The next band $D$ has its maximum at 403.24 eV (Table II) with a TV of 2.06 eV and was assigned [6] to the transition to a $\sigma^*$ (NH$_2$) state. For TV's below 2 eV, the calculations of Table III predict a large number of transitions, most of them being pure Rydberg states with very low intensities. A few states have larger intensities, because of a mixed Rydberg-valence character of the transition: the N $1s$ $\rightarrow 3d\sigma/\sigma^*$ (NH$_2$) transition, calculated with a TV of 1.73 eV, could be responsible for the 403.24-eV feature. The N $1s \rightarrow 4p\sigma/\sigma^*$ (NH$_2$) and N $1s \rightarrow 4p\pi/2\pi^*$ ($4b_1$) transitions are also rather intense and contribute to the intensity in this energy region.

At higher energies, the Rydberg transitions converge to the continuum onset corresponding to the ionization energy,

calculated at 405.47 eV. A simple way to test the accuracy of the calculated Rydberg transitions is to perform a quantum defect analysis using the well-known Rydberg formula:

$$E(1s \rightarrow n\ell) = E(1s \rightarrow \infty) - \frac{R}{(n - \delta_\ell)^2},$$

where $R$ is the Rydberg constant, $n$ is the principal quantum number, and $\delta_\ell$ is the quantum defect. Table IV shows the results of a fitting procedure using the calculated values of Table III. For $s$ and $p$ transitions, the fitted ionization potential (IP's), located between 405.38 and 405.45 eV, are close to the experimental value [31] of 405.3 eV and consistent with the CIPSI value of 405.47 eV.

According to the calculations, the two N $1s \rightarrow \sigma^*$ (NH$_2$) have TV's close to zero and lie at the ionization continuum onset. One of these transitions ($B_2$ symmetry) has the largest intensity of the whole spectrum. It is highly probable that this proximity to the continuum induces a very short lifetime for these transitions. Consequently, the corresponding bands have probably large full width at half maximum (FWHM) which might explain the flatness of the observed spectrum around 405 eV (Figs. 2 and 3).

The last two bands $E$ and $F$ can be seen in the experimental spectrum at higher energies (Fig. 2) at 406.1 eV (TV=−0.8 eV) and 407.6 eV (TV=−2.3 eV). Above the ionization threshold, the present calculations may not be quantitatively accurate, since they do not take into account the coupling with the continuum states. According to Table IV, the $E$ band could be due to the N $1s \rightarrow 3\pi^*$ and N $1s \rightarrow \sigma^*$ (C$_3$H) transitions. The N $1s \rightarrow 3\pi^*$ ($5b_1$) state is strongly mixed with a large number of di-excitations and there is also a doubly excited state with small $3\pi^*$ character calculated at 408.40 eV. A natural population analysis [38] shows without ambiguity that the 406.60-eV transition is essentially monoelectronic. A similar mixing also occurs for the N $1s \rightarrow \sigma^*$ (C$_3$H) transition. For band $F$ there is very likely also a contribution from shape resonances, although this type of assignment has been questioned [39].

In Fig. 3, the experimental spectrum is compared with the calculated one. It should be noticed that all calculated bands have been taken into account, including the low intensity transitions not shown in Table IV. There is good agreement between both sets of data, except from a slight overestimation ($\sim$0.5 eV) of the calculated values, as already stated before. It should be noticed that the STEX results of Carravetta *et al.* (Fig. 4 of Ref. [8]) were overestimated by
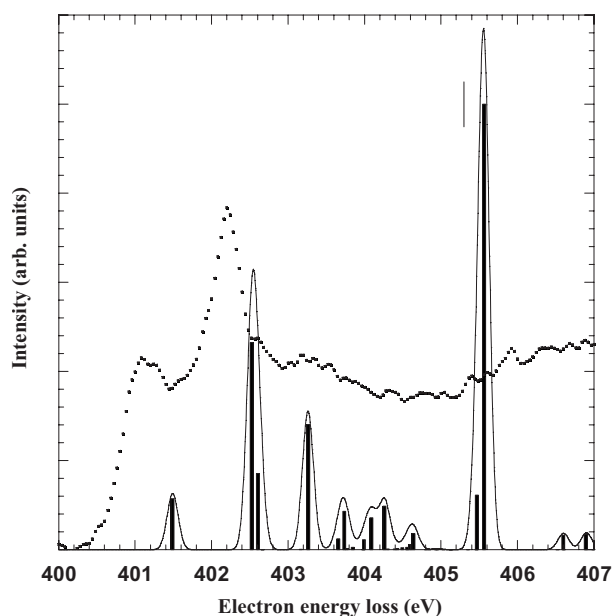
FIG. 3. Comparison between the experimental and the theoretical spectra for the pre-edge region at the nitrogen *K*-edge. The calculated results are convoluted by the experimental profile with 0.17 eV as the bandwidth at half maximum. The vertical lines show the measured ionization threshold.

~1.2 eV with respect to the spectrum of Turci *et al.* [6]. This figure also shows that the 0.17-eV bandwidth used is too narrow to reproduce the observed spectrum, the most part of the broadness of the experimental bands being due to the short lifetimes of the excited species.

### C. Carbon *K*-shell electron energy-loss spectrum

The experimental excitation spectrum at the C 1*s* edge is presented in Fig. 4. It is quite similar to that of Turci *et al.*

[6], some fine features being better resolved thanks to the higher resolution in the present study. The energy values of the observed spectral bands are given in Table V and are compared to previous studies on gaseous aniline but also on samples condensed on metallic substrates. The table also provides the assignments proposed previously for the gas phase spectra. In Table VI the results of the calculations are given. Only the transitions with intensities larger than 1.5% of the most intense band are shown, except for $A_2$ transitions. For the assignment of the spectrum, one has to keep in mind that the calculated values are probably slightly overestimated (see Fig. 5). Contrary to the nitrogen case, using TV values is more difficult, because of the four nonequivalent carbon atoms.

The first band *A*, the most intense one, is observed at 285.29 eV (Table V) and is assigned without ambiguity to the excitation of the $2\pi^*$ molecular orbital from $C_2$ 1*s*, $C_3$ 1*s*, and $C_4$ 1*s* which are calculated to be nearly degenerate, respectively, at 285.52, 285.53, and 285.64 eV as shown in Table VI. The largest intensity predicted is for $C_3$ $1s \rightarrow 2\pi^*$. These results are consistent with the experimental broadness of the spectral band (Fig. 4) which has a FWHM of about 0.9 eV. Table VII compares the present calculations to previous theoretical studies. With the exception of the EHMO values of Turci *et al.* [6], which are underestimated by several eV, all results are slightly too high. Table VIII confirms that $C_2$ $1s \rightarrow 2\pi^*$ and $C_3$ $1s \rightarrow 2\pi^*$ transitions are almost perfectly degenerate, because they are less perturbed by the substitution of a hydrogen atom by the amino group when going from benzene to aniline. On the other hand, the chemical shifts are more important for $C_4$ and of course for $C_1$. They appear to be smaller than their equivalent in the core ions (Table I).

The band *B* has its maximum of intensity at 286.69 eV and is highly asymmetric on the high-energy side with a not well resolved feature *C* at 286.88 eV as shown in the inset of Fig. 4. Feature *C* is not mentioned by Turci *et al.*, very likely
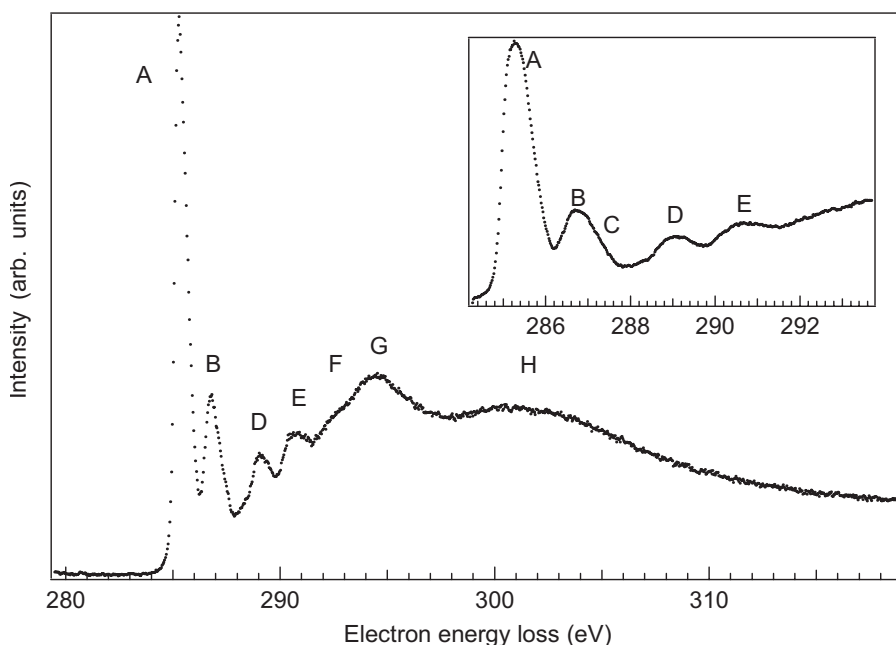


FIG. 4. The electron energy-loss spectrum of aniline recorded at the carbon *K*-edge with an energy resolution of 0.17 eV, steps of 40 meV. Inset: lowest energy region recorded with 20-meV steps.

TABLE V. Experimental energy values (eV) of the spectral bands in the C 1s excitation spectrum of aniline and previous proposed assignments.

| Band | $E$ (eV)[a] gas | $E$ (eV)[b] gas | $E$ (eV)[c] solid | $E$ (eV)[d] solid | Assignments[b] (C-H) $C_1, C_2, C_3$ | (C-N) $C_4$ |
|------|------|------|------|------|------|------|
| A | 285.29 | 285.2 | 285.4 | 285.4 | $2\pi^*$ ($4b_1$) | |
| B | 286.69 | 286.7 | 286.9 | 286.8 | | $2\pi^*$ ($4b_1$) |
| C | 286.88 | | | | | |
| D | 289.11 | 289.0 | 288.7 | | $3\pi^*$ ($5b_1$)/3p | |
|   | (290.2) | | | | | |
| E | 290.65 | 290.5 | 290.6 | | | $3\pi^*$ ($5b_1$)/$\sigma^*$ ($CNH_2$) |
| F | 292.3 | | | | | |
| G | 294.5 | 294.5 | 294.5 | | | $1\sigma^*$ |
| H | 301 | 3.2 | $303 \pm 1.0$ | | | $2\sigma^*$ |

[a]This work.
[b]Reference [6].
[c]Reference [3].
[d]Reference [5].

being not resolved at all in their spectrum. The *B* band has been assigned to the $C_4$ $1s \rightarrow 2\pi^*$ ($4b_1$) [6]. The calculations support this assignment, since the $C_1$ $1s \rightarrow 2\pi^*$ ($4b_1$) transition is predicted to occur at a slightly higher energy of 287.16 eV (Table VIII). This transition has also the highest intensity of all. The calculations also reveal the presence of many other transitions in this energy region. Some of them, being purely Rydberg, are not shown in Table VI. For $C_2$, $C_3$, and $C_4$, the transitions to the $3s\sigma$ MO are predicted at very close energies (between 286.79 and 287.07 eV). Their relatively high intensity (about 4% of the most intense peak) is due to their $\sigma^*$ (CH) valence character. The corresponding transition $C_1$ $1s \rightarrow 3s\sigma/\sigma^*(NH_2)$ (not shown in Table VI) is calculated at 288.48 eV but with a very small intensity (0.3%). The four transitions have nearly identical TV's, around 3 eV.

The calculated transitions to the $1\pi^*$ exhibit the same patterns as the $2\pi^*$ and $3s\sigma$ transitions for the four atoms: the $C_2$, $C_3$, and $C_4$ transitions occur between 285.90 and 286.59 eV, while the $C_1$ transition is calculated at 287.48 eV. There are, however, differences in the wave functions: for $C_1$ and $C_4$, the wave function is purely $1\pi^*$, while for $C_2$ and $C_3$, there is a mixing between $1\pi^*$ and $3p\pi$ and $3d\pi$ configurations. This mixing is due to the fact that $C_2$ and $C_3$ were calculated in $C_s$ symmetry while $C_{2v}$ symmetry was used for $C_1$ and $C_4$. It is also interesting to note that the $C_2$ and $C_3$ transitions have very weak intensities. This would tend to confirm that the two $A_2$ transitions would have also weak intensities in the nonplanar geometry.

The band *D* is observed with a maximum intensity at 289.11 eV. It presents fine features not well resolved on the low-energy side at 288.37 eV and on the high-energy side at 289.43 eV. It has been reported previously [3,6] and assigned to excitation of $3\pi^*$ ($5b_1$) or 3p MO's [6] or possibly $\sigma^*$ (CH) MO [3] from $C_2$, $C_3$, or $C_4$ atoms. Plashkevych *et al.* [7] noticed that the experimental TV would suggest a 4p rather than 3p transition in this region. The present calcula-

tions show that there are many $n=4$ and 5 Rydberg transitions from $C_1$, $C_2$, and $C_3$ in this energy region. Most of them have very low intensities and are not shown in Table VI. They contribute to the intensity on the low-energy side of the *D* band. In fact, according to the calculations, the *D* band appears to be due to the excitation to the $3\pi^*$ MO form $C_2$ and $C_4$ and, to a lesser extent, from $C_3$ in the low-energy side. As for N and $C_4$, the wave functions appear to be a mixing between $3\pi^*$ and valence $1s$ $\pi \rightarrow \pi^*$ $\pi^*$ di-excited configurations. Because of their $\langle r^2 \rangle$ value around 90 a.u.$^2$, they clearly have valence character. The configuration mixing might reflect the fact that the $3\pi^*$ virtual MO of the core ion is not the best one to describe the core excitation, but it may also indicate the presence of a true high intensity shake-up state, as we have found recently in the N 1s $K$ shell of $s$-triazine [40]. This is especially true for $C_3$, since there are two states (calculated at 288.83 and 289.82 eV) with an important $3\pi^*$ character (19 and 27 %) mixed with di-excitations. In order to define the mono- or di-excited character of this type of states, a natural orbital analysis [38] was performed. The resulting fractional occupation numbers show that for $C_2$, $C_3$, and $C_4$, there are about 1.5 electrons in $\pi^*$ MO's, corresponding to an intermediate situation between mono- and di-excited states. With a population of 1.8 electrons in $\pi^*$ and about 0.9 electron removed from the $\pi$ MO's, the second $C_3$ $3\pi^*$ state may be viewed as a "true" shake-up state.

The next band *E* is located at 290.65 eV as shown in Fig. 4 and is between the $C_2$, $C_3$, $C_4$ ionization threshold and the $C_1$ one. Previously it has been assigned to $3\pi^*$ ($5b_1$) [3,6] or $\sigma^*$ ($CNH_2$) [3,6,7] (Table V). The calculations predict an intense transition at 290.88 eV involving the $C_1$ $1s \rightarrow 3\pi^*$ transition with an important (20%) $2\pi$ $C_1$ $1s \rightarrow 1\pi^*2\pi^*$ character. According to the natural MO's analysis, it may be considered as monoelectronic since there is 1.1 electron in $\pi^*$ MO's. There are also $\sigma^*$ and shake-up transitions in this energy range but their intensities are low. The quasidegener-

TABLE VI. Calculated energies, TV's, relative intensities, and assignments at the C 1s different core shell of aniline.

| State | $E$ (eV) | TV (eV) | | | | Intensity[a] | Main configurations[b] | $\langle r^2 \rangle$ |
|---|---|---|---|---|---|---|---|---|
| | | $C_1$ | $C_2$ | $C_3$ | $C_4$ | | | |
| $A''$ | 285.52 | | 4.47 | | | 0.588 | 0.91 $C_2$ 1s→2π* (4b₁) | 90 |
| $A''$ | 285.53 | | | 4.59 | | 0.803 | 0.90 $C_3$ 1s→2π* (4b₁) | 88 |
| $B_1$ | 285.64 | | | | 4.14 | 0.645 | 0.89 $C_4$ 1s→2π* (4b₁) | 88 |
| $A_2$ | 285.90 | | | | 3.89 | 0.000[c] | 0.92 $C_4$ 1s→1π* (2a₂) | 89 |
| $A''$ | 286.59 | | | 3.53 | | 0.029 | 0.58 $C_3$ 1s→1π* (2a₂) +0.13 $C_3$ 1s→3pπ | 90 |
| $A_1$ | 286.79 | | | | 2.99 | 0.041 | 0.95 $C_4$ 1s→3sσ/σ* (C₄H) | 160 |
| $A'$ | 286.84 | | 3.15 | | | 0.047 | 0.97 $C_2$ 1s→3sσ/σ* (C₂H) | 157 |
| $A'$ | 287.07 | | | 3.06 | | 0.043 | 0.96 $C_3$ 1s→3sσ/σ* (C₃H) | 161 |
| $B_1$ | 287.16 | 4.36 | | | | 1.000[d] | 0.91 $C_1$ 1s→2π* (4b₁) | 91 |
| $A_2$ | 287.48 | 4.04 | | | | 0.000[c] | 0.92 $C_1$ 1s→1π* (2a₂) | 92 |
| $A_1$ | 287.93 | | | | 1.85 | 0.015 | 0.93 $C_4$ 1s→3dσ | 215 |
| $A''$ | 288.03 | | | 2.10 | | 0.017 | 0.82 $C_3$ 1s→3pπ +0.15 $C_3$ 1s→1π* (2a₂) | 208 |
| $B_1$ | 288.28 | | | | 1.51 | 0.037 | 0.98 $C_4$ 1s→3dπ | 292 |
| $A_2$ | 288.33 | | | | 1.46 | 0.000[c] | 0.98 $C_4$ 1s→3dπ' | 308 |
| $A_1$ | 288.39 | | | | 1.40 | 0.015 | 0.94 $C_4$ 1s→4sσ | 550 |
| $A'$ | 288.49 | | 1.50 | | | 0.019 | 0.98 $C_2$ 1s→4sσ | 510 |
| $A'$ | 288.68 | | | 1.44 | | 0.016 | 0.97 $C_3$ 1s→4sσ | 551 |
| $B_1$ | 288.79 | | | | 0.99 | 0.040 | 0.98 $C_4$ 1s→4dπ | 604 |
| $A''$ | 288.83 | | | 1.29 | | 0.064 | 0.19 $C_3$ 1s→3π* (5b₁) +0.58 3π $C_3$ 1s→2π* (4b₁) 2π* (4b₁) | 88 |
| $A_2$ | 288.83 | | | | 0.96 | 0.000[c] | 0.98 $C_4$ 1s→4dπ' | 552 |
| $A''$ | 288.98 | | | 1.14 | | 0.017 | 0.93 $C_3$ 1s→4pπ | 774 |
| $A''$ | 289.36 | | 0.63 | | | 0.137 | 0.54 $C_2$ 1s→3π* (5b₁) +0.19 3π $C_2$ 1s→2π* (4b₁) 2π* (4b₁) | 85 |
| $B_1$ | 289.42 | | | | 0.36 | 0.166 | 0.58 $C_4$ 1s→3π* (5b₁) +0.17 2π $C_4$ 1s→1π* (2a₂) 2π* (4b₁) | 91 |
| | 289.79 | | | | 0.00 | | Ion $C_4$ | |
| $A''$ | 289.82 | | | 0.30 | | 0.027 | 0.27 $C_3$ 1s→3π* (5b₁) +0.20 3π $C_3$ 1s→2π* (4b₁) 2π* (4b₁) +0.26 3π $C_3$ 1s→1π* (2a₂) 2π* (4b₁) | 95 |
| $A_2$ | 289.98 | 1.54 | | | | 0.000[c] | 0.98 $C_1$ 1s→3dπ | 274 |
| | 289.99 | | 0.00 | | | | Ion $C_2$ | |
| $A_1$ | 290.06 | | | | −0.27 | 0.040 | 0.94 $C_4$ 1s→σ* (C₂H) | 142 |
| | 290.13 | | | 0.00 | | | Ion $C_3$ | |
| $A''$ | 290.35 | | −0.35 | | | 0.018 | 0.30 3π $C_2$ 1s→2π* (4b₁) 2π* (4b₁) +0.37 3π $C_2$ 1s→2π* (4b₁) 3pπ | 142 |
| $A_2$ | 290.53 | 0.99 | | | | 0.000[c] | 0.98 $C_1$ 1s→4dπ | 576 |
| $A''$ | 290.73 | | −0.74 | | | 0.027 | 0.24 3π $C_2$ 1s→2π* (4b₁) 2π* (4b₁) +0.37 3π $C_2$ 1s→2π* (4b₁) 3pπ | 166 |
| $B_1$ | 290.88 | 0.64 | | | | 0.255 | 0.56 $C_1$ 1s→3π* (5b₁) +0.20 2π $C_1$ 1s→1π* (2a₂) 2π* (4b₁) | 103 |
| $B_1$ | 291.37 | 0.15 | | | | 0.047 | 0.54 3π $C_1$ 1s→2π* (4b₁) 2π* (4b₁) +0.24 2π $C_1$ 1s→1π* (2a₂) 2π* (4b₁) | 96 |
| | 291.52 | 0.00 | | | | | Ion $C_1$ | |
| $A_1$ | 291.56 | −0.04 | | | | 0.036 | 0.91 $C_1$ 1s→σ* (CH) | 159 |
| $B_2$ | 291.80 | | | | −2.01 | 0.018 | 0.95 $C_4$ 1s→σ* (C₃H) | 125 |
| $B_2$ | 291.97 | −0.44 | | | | 0.033 | 0.93 $C_1$ 1s→σ* (NH₂) | 121 |

[a]Relative intensity to the most intense band.
[b]Main configuration of the CI wave function.
[c]Dipole-electric forbidden transition.
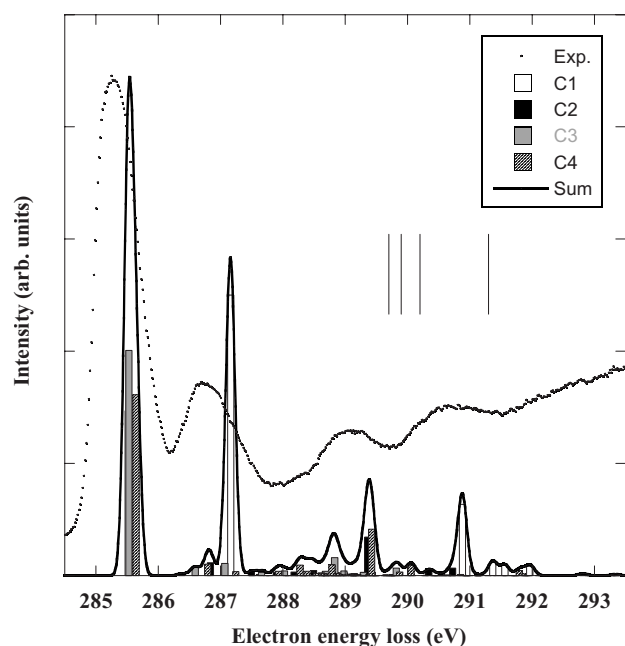[d]Absolute calculated oscillator strengths (length gauge): $f_L = 0.0525$.

FIG. 5. Comparison between the experimental and the theoretical spectra at the carbon *K*-edge. The calculated results are convoluted by the experimental profile with 0.17 eV as the bandwidth at half maximum and compared to the experimental spectrum. The vertical lines show the measured ionization thresholds.

ate continuum onsets are probably responsible for the large width of this band.

The *F* feature at 292.3 eV appears as a shoulder on band *G*. It is above the $C_1$ ionization threshold. In this energy region there are several bands with rather small intensities predicted by the calculations, involving $\sigma^*$ and shake-up transitions. At higher energy as shown in Fig. 4 there are two broad bands with maximum of intensity at 294.5 and 301 eV also reported previously and assigned to $\sigma^*$ type excitation (Table V). They are tentatively assigned to shape resonances [39].

As shown in Table IV, it is also possible to perform a quantum defect analysis on the Rydberg states of the four carbon atoms. For *s* and *p* transitions, all atoms give very similar $\delta_\ell$ values and the fitted ionization potentials are consistent with the calculated CIPSI value. Finally, Fig. 5 compares the experimental spectrum with the calculated bands. The upper spectrum shows the contributions of all carbon

atoms to the spectrum, the result of the calculations being fitted with 0.17-eV FWHM Gaussians. It should be noticed that all calculated bands have been taken into account, including the low intensity transitions not shown in Table VI. There is an excellent agreement for the relative intensities and the calculated energies seem to be slightly overestimated by a few tenths of an eV. In the STEX calculations of Plashkevych *et al.* [Fig. 7(a) of [7]], the calculated spectrum was shifted by 1.52 eV to match the experiment of Turci *et al.* [6].

### D. Geometry of core excited aniline

Due to variational collapse of the wave function, geometry optimization of the core states of polyatomic molecules is a difficult task [41–43], especially at the multiconfigurational level. In the case of benzene, Norman and Ågren [44] optimized the geometry of the core ion, the C $1s \rightarrow 1\pi^*$ ($1e_{2u}$) core state, and its equivalent core ($Z+1$) [45], using a double-dzeta quality basis state and an active space limited to $\pi$ MO's. It was shown that these three states remained planar, in contradiction with early suggestions of a pyramidalized structure [46]. On the whole, the equivalent core approximation geometry and frequencies were very close to the true core results, except for the lowest frequencies ("soft" modes).

In the case of aniline, it is interesting to study how the substitution of a $NH_2$ group in benzene could affect the geometry of the core excited molecule. These calculations were performed with the GAMESS-US program at the ROHF-GVB level [47], using the TZP+$R$ basis set. The nature (minima or saddle points) of the structures was determined by calculating analytically the harmonic frequencies at the same level. The various geometries obtained can be classified in six main types, displayed in Figs. 1(a)–1(f). The results of the calculations are summarized in Table VIII, while the detailed structural parameters are provided in the supplementary data of this paper [30]. Briefly, the changes in bond lengths are consistent with the findings of Norman and Ågren [44] for benzene: the core excited C-H length is shortened to a value close to a N-H bond (about 1.0 Å). Similarly, the core excited N-H bond is shortened to the typical O-H value (about 0.96 Å). When the 1*s* electron is excited to a Rydberg MO with $\sigma^*$ (C-H) valence character, this shortening is counterbalanced by a slight increase of the bond length. Bond angles

TABLE VII. Transition energies of the most intense bands in carbon 1*s* excitation spectrum at different levels of theory.

| | CIPSI[a] | Shift[a] | STEX[b] | Shift[b] | $\Delta$SCF[b] | Shift[b] | Shift[c] | EHMO[d] | Shift[d] | Expt.[a] | Shift[a] |
|---|---|---|---|---|---|---|---|---|---|---|---|
| $C_1$ | 287.16 | 1.63 | 287.23 | 1.45 | 287.69 | 1.46 | 1.15 | 282.1 | 1.15 | 286.61 | 1.32 |
| $C_2$ | 285.52 | −0.01 | 285.68 | 0.09 | 286.31 | 0.08 | 0.03 | 281.0 | 0.03 | | $\approx$0.0 |
| $C_3$ | 285.53 | 0.00 | 285.78 | 0.00 | 286.23 | 0.00 | 0.00 | 280.8 | 0.00 | 285.29 | 0.0 |
| $C_4$ | 285.64 | 0.11 | 285.89 | 0.11 | 286.51 | 0.28 | 0.29 | 281.2 | 0.40 | | $\approx$0.0 |

[a]This work.
[b]Reference [8].
[c]MCSCF values from Ref. [5].
[d]Reference [6].

TABLE VIII. Core ionized and excited states of aniline and $Z+1$ equivalent molecules.

| | Core | | | Z+1 | | |
|---|---|---|---|---|---|---|
| | State | Figure | $n_i^a$ | State | Figure | $n_i^a$ |
| Ion $C_1$ | $^2A'$ | 1(d) | 0 | $^1A'$ | 1(d) | 0 |
| Ion $C_2$ | $^2A'$ | 1(c) | 0 | $^1A'$ | 1(c) | 0 |
| Ion $C_3$ | $^2A$ | 1(d) | 0 | $^1A$ | 1(d) | 0 |
| Ion $C_4$ | $^2A_1$ | 1(c) | 0 | $^1A_1$ | 1(c) | 0 |
| Ion N | $^2A_1$ | 1(b) | 0 | $^1A'$ | 1(d) | 0 |
| $C_1$ $1s \rightarrow 3s\sigma/\sigma^*$ (NH$_2$) | $^1A'$ | 1(d) | 0 | $^2A'$ | 1(d) | 0 |
| $C_1$ $1s \rightarrow 2\pi^*$ ($4b_1$) | $^1A$ | 1(d)$^b$ | 0 | $^2A$ | 1(d)$^b$ | 0 |
| $C_2$ $1s \rightarrow 3s\sigma/\sigma^*$ (C$_2$H) | $^1A'$ | 1(c) | 0 | $^2A'$ | 1(c) | 0 |
| $C_2$ $1s \rightarrow 1\pi^*$ ($2a_2$) | $^1A$ | 1(e) | 0 | $^2A$ | 1(e) | 0 |
| $C_3$ $1s \rightarrow 3s\sigma/\sigma^*$ (C$_3$H) | $^1A'$ | 1(c) | 1 | $^2A'$ | 1(c) | 1 |
| $C_3$ $1s \rightarrow 1\pi^*$ ($2a_2$) | $^1A$ | 1(f) | 0 | $^2A$ | 1(f) | 0 |
| $C_4$ $1s \rightarrow 2\pi^*$ ($4b_1$) | $^1B_1$ | 1(c) | 0 | $^2B_1$ | 1(c) | 0 |
| $C_4$ $1s \rightarrow 3p\sigma/\sigma^*$ (CH) | $^1B_2$ | 1(c) | 0 | $^2B_2$ | 1(c) | 0 |
| $C_4$ $1s \rightarrow 3s\sigma/\sigma^*$ (C$_4$H) | $^1A_1$ | 1(c) | 0 | $^2A_1$ | 1(c) | 0 |
| $C_4$ $1s \rightarrow 1\pi^*$ ($2a_2$) | $^1A''$ | 1(a) | 0 | $^2A''$ | 1(a) | 0 |
| N $1s \rightarrow 3s\sigma/\sigma^*$ (NH$_2$) | $^1A'$ | 1(d) | 0 | $^2A'$ | 1(d) | 0 |
| N $1s \rightarrow 3p\sigma$ | $^1B_2$ | 1(b) | 0 | $^2A''$ | 1(d) | 0 |
| N $1s \rightarrow 3p\pi/\sigma^*$ (NH$_2$) | $^1B_1$ | 1(b) | 0 | $^2B_1$ | 1(b) | 1 |
| N $1s \rightarrow 1\pi^*$ ($2a_2$) | $^1A_2$ | 1(b) | 2 | $^2A_2$ | 1(b) | 1 |

$^a$Number of imaginary frequencies.
$^b$Slightly distorted from the $C_s$ geometry (C$_1$-N bond out of ring plane).

generally remain close to 120°. These trends are also valid for the $Z+1$ molecules.

However, as indicated in Table VIII, it appears that most core states do not have the geometry of the ground state [Fig. 1(a)]. Core ions are either planar [$C_1$, $C_4$, Fig. 1(c)] or the amino group is rotated by 90° from the ring plane [$C_2$, $C_4$, Fig. 1(c)]. For N, there is a discrepancy between the core ion predicted to have the geometry of Fig. 1(b), while the $Z+1$ approximation predicts the geometry shown in Fig. 1(d). Since the rotation of the NH$_2$ group has the lowest frequency, these results confirm the prediction of Norman and Ågren [44].

For core excited aniline, it was possible to optimize at least two states for each carbon atom. For $C_4$, which is the farthest from the amino group, and thus similar to benzene, the $C_4$ $1s \rightarrow 1\pi^*$ ($2a_2$) core state keeps the geometry of the ground state, while the $C_4$ $1s \rightarrow 2\pi^*$ ($4b_1$) state is planar. On the other hand, for $C_2$ and $C_4$, the same transition leads to a pyramidalized structure [Figs. 1(e) and 1(f)]. For $C_1$, the lowest transition is the $\pi^*$ ($3b_1$) and corresponds to Fig. 1(d) but with the C$_1$-N bond slightly out of the ring plane. Most of the Rydberg-$\sigma^*$ (CH) states are planar. For carbons, there is a perfect agreement between core states and their $Z+1$ equivalent.

For nitrogen, the N $1s \rightarrow 3s\sigma/\sigma^*$ (NH$_2$) has the geometry of Fig. 1(d), while the two $3p\sigma$ states have the 90° rotated structure of Fig. 1(b). The N $1s \rightarrow 1\pi^*$ ($2a_2$) state could not be found (the planar form had three imaginary frequencies and the nonplanar structures correspond to other transitions)

but has probably the Fig. 1(d) geometry. As for the core ion, there are some discrepancies between the core states and their $Z+1$ equivalent concerning the nature of the calculated structures. These discrepancies, which are due to the valence to core penetration neglected in the $Z+1$ approximation [43], would be more important for nitrogen than for carbon, leading to different geometries. Geometry optimizations on species containing both carbon and oxygen atoms [48] show similar trends, while for cyclopropane, the $Z+1$ structures and energies were found to be very close to the core states [43].

## V. CONCLUSIONS

The C 1$s$ and N 1$s$ electron energy-loss spectra have been recorded by electron impact under electric dipole interaction conditions and with higher resolution than previously. Accompanying *ab initio* configuration interaction calculations have been performed in order to propose quite reliable assignments.

The transitions to the lowest energy unoccupied MO's of $\pi^*$ type from the carbon atoms $C_2$, $C_3$, $C_4$ are nearly degenerate. They are separated by about 1.6 eV from the $C_1$ 1$s$ $\rightarrow 2\pi^*$. This suggests that the carbon atoms $C_2$, $C_3$, and $C_4$ have roughly the same chemical environment and that of $C_1$ is about 1.6 eV different and shifting the spectral bands at higher energy. At the N 1$s$ edge the most intense transitions are due to the strong Rydberg-valence states, involving the $\sigma^*$-type unoccupied molecular orbitals.

Some discrepancies between the N 1$s$ excited core states and their $Z+1$ equivalent concerning the nature of their equilibrium geometries are observed. It is not the case for the carbons for which there is an excellent agreement between core states and their $Z+1$ equivalent. These differences, being due to the valence to core penetration neglected in the $Z+1$ approximation, seem to be more important for nitrogen than for carbon.

[1] M. Magnuson *et al.*, J. Chem. Phys. **111**, 4756 (1999).

[2] N. E. Agbor *et al.*, Sens. Actuators B **41**, 137 (1997).

[3] J. L. Solomon, R. J. Madix, and J. Stohr, Surf. Sci. **255**, 12 (1991).

[4] J. Stöhr, *NEXAFS Spectroscopy* (Springer-Verlag, Berlin, 1992).

[5] Y. Luo *et al.*, Phys. Rev. A **52**, 3730 (1995).

[6] C. C. Turci, S. G. Urquhart, and A. P. Hitchcock, Can. J. Chem. **74**, 851 (1996).

[7] O. Plashkevych *et al.*, Chem. Phys. **222**, 125 (1997).

[8] V. Carravetta, O. Plashkevych, and H. Ågren, Chem. Phys. **263**, 231 (2001).

[9] C. Hannay *et al.*, Meas. Sci. Technol. **6**, 1140 (1995).

[10] M.-J. Hubin-Franskin *et al.*, J. Chem. Phys. **106**, 35 (1997).

[11] M.-J. Hubin-Franskin and J. Heinesch, Nucl. Instrum. Methods Phys. Res. A **477**, 546 (2002).

[12] R. N. S. Sodhi and C. E. Brion, J. Electron Spectrosc. Relat. Phenom. **34**, 363 (1984).

[13] D. Duflot *et al.*, J. Chem. Phys. **118**, 1137 (2003).

[14] S. Bodeur, P. Millié, and I. Nenner, Phys. Rev. A **41**, 252 (1990).

[15] M. W. Schmidt *et al.*, J. Comput. Chem. **14**, 1347 (1993).

[16] B. Huron, J. P. Malrieu, and P. Rancurel, J. Chem. Phys. **58**, 5745 (1973).

[17] R. Cimiraglia, J. Chem. Phys. **83**, 1746 (1985).

[18] C. Angeli *et al.*, Theor. Chem. Acc. **98**, 57 (1997).

[19] T. H. Dunning, Jr., J. Chem. Phys. **55**, 716 (1971).

[20] T. H. Dunning, Jr. and P. J. Hay, in *Methods of Electronic Structure Theory*, edited by H. F. Schaefer III (Plenum Press, New York, 1977), Vol. 3, p. 1.

[21] D. G. Lister and J. K. Tyler, Chem. Commun. (London) **6**, 152 (1966).

[22] D. G. Lister *et al.*, J. Mol. Struct. **23**, 253 (1974).

[23] N. W. Larsen, E. L. Hansen, and F. M. Nicolaisen, Chem. Phys. Lett. **43**, 584 (1976).

[24] M. Quack and M. Stockburger, J. Mol. Spectrosc. **43**, 87 (1972).

[25] J. Pyka and M. Kreglewski, J. Mol. Spectrosc. **109**, 207 (1985).

[26] O. Bludský *et al.*, J. Chem. Phys. **105**, 11042 (1996).

[27] M. Alcolea Palafox, J. L. Nunez, and M. Gil, J. Mol. Struct.: THEOCHEM **593**, 101 (2002).

[28] Y. Honda *et al.*, J. Chem. Phys. **117**, 2045 (2002).

[29] P. M. Wojciechowski, W. Zierkiewicz, and D. Michalska, J. Chem. Phys. **118**, 10900 (2003).

[30] See EPAPS Document No. E-PLRAAN-75-069704 for detailed structural and energy information on the ground, core ion, and core excited states of aniline. For more information on EPAPS, see http://www.aip.org/pubservs/epaps.html

[31] T. Ohta, T. Fujikawa, and H. Kuroda, Bull. Chem. Soc. Jpn. **48**, 2017 (1975).

[32] T. D. Crawford, H. F. Schaefer III, and T. J. Lee, J. Chem. Phys. **105**, 1060 (1996).

[33] P. J. Knowles *et al.*, Chem. Phys. Lett. **186**, 130 (1991).

[34] W. J. Lauderdale *et al.* Chem. Phys. Lett. **187**, 21 (1991).

[35] T. J. Lee *et al.* J. Chem. Phys. **100**, 7400 (1994).

[36] T. J. Lee and D. Jayatilaka, Chem. Phys. Lett. **201**, 1 (1993).

[37] E. Shigemasa *et al.*, Phys. Rev. A **66**, 022508 (2002).

[38] P.-O. Löwdin, Phys. Rev. **97**, 1474 (1955).

[39] M. N. Piancastelli, J. Electron Spectrosc. Relat. Phenom. **100**, 167 (1999).

[40] D. Duflot *et al.*, Eur. Phys. J. D **35**, 239 (2005).

[41] S. Shirai, S. Yamamoto, and S.-a. Hyodo, J. Chem. Phys. **121**, 7586 (2004).

[42] A. B. Trofimov *et al.*, J. Chem. Phys. **113**, 6716 (2000).

[43] D. Duflot, S. Zeggari, and J.-P. Flament, Chem. Phys. **327**, 518 (2006).

[44] P. Norman and H. Ågren, J. Mol. Struct.: THEOCHEM **401**, 107 (1997).

[45] W. L. Jolly and D. N. Hendrickson, J. Am. Chem. Soc. **92**, 1863 (1970).

[46] Y. Ma *et al.*, Phys. Rev. Lett. **63**, 2044 (1989).

[47] G. Chaban, M. W. Schmidt, and M. S. Gordon, Theor. Chem. Acc. **97**, 88 (1997).

[48] D. Duflot *et al.* (unpublished).